

SWINBURNE UNIVERSITY OF TECHNOLOGY



---

## HAND-EYE COORDINATION REPORT

---

RME 40003

### ROBOT SYSTEM DESIGN

---

Justin Sargent 9989900

Phillip Smith 7191731

Thomas Rappos 6336361

---

# Contents

|          |  |           |
|----------|--|-----------|
| <b>1</b> | <b>Project Outline</b>                         | <b>2</b>  |
| <b>2</b> | <b>Computer Vision</b>                         | <b>3</b>  |
| 2.1      | Camera use . . . . .                           | 3         |
| 2.2      | Object detection . . . . .                     | 3         |
| 2.2.1    | Environment preparation . . . . .              | 3         |
| 2.2.2    | Object recognition . . . . .                   | 3         |
| 2.2.3    | Object orientation . . . . .                   | 6         |
| 2.3      | Pin detection and PinHole Allocation . . . . . | 6         |
| 2.4      | Path creation . . . . .                        | 9         |
| 2.4.1    | Pinhole and gripper location . . . . .         | 9         |
| 2.4.2    | Measurement correction . . . . .               | 10        |
| 2.4.3    | Path to gripper arm co-ordinates . . . . .     | 10        |
| 2.4.4    | Error correction . . . . .                     | 11        |
| 2.5      | Camera future development suggested . . . . .  | 12        |
| <b>3</b> | <b>Robotic Arm Control</b>                     | <b>13</b> |
| 3.1      | Open ABB . . . . .                             | 13        |
| 3.2      | Coordination . . . . .                         | 13        |
| 3.3      | Pin placement operation . . . . .              | 14        |
| <b>4</b> | <b>Operation Flow</b>                          | <b>15</b> |
| <b>5</b> | <b>Matlab Simulation</b>                       | <b>18</b> |
| 5.1      | Denavit-Hartenberg Algorithm . . . . .         | 18        |
| 5.2      | Matlab implementation . . . . .                | 18        |
| <b>A</b> | <b>Matlab Code</b>                             | <b>20</b> |

# Chapter 1

## Project Outline

This project explores the use of a robotic arm used for pick-and-place automation tasks. For dynamic operation and task-completion feed-back, computer vision is incorporated via a web-cam mounted in the work area.

More specifically, this project has been completed for an industry client, AME System Pty. Ltd., for automated cavity pin insertion. These pins are 3.5mm wide and are placed in holes between 5 and 9mm apart on a rubber socket, as shown in fig. 1.1(a) Due to this small size, a high degree of accuracy and repeatability is required.

To hold the socket in place, and determine the orientation, a holding box has been

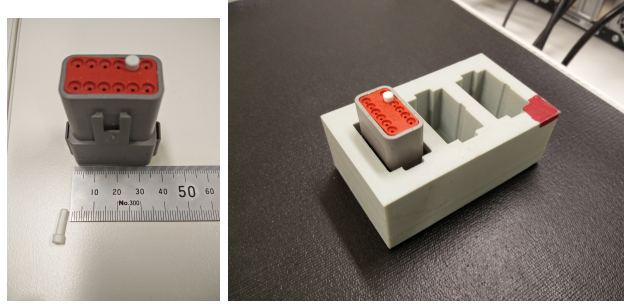


Figure 1.1: Image of pin and socket, and socket in holding box

produced which slots the sockets into a fixed position, shown in fig. 1.1(b). For this project, these boxes are not themselves placed in a fixed location within the work space. This allows easy setup for human operators; they can simply place a holding box full of unfilled sockets anywhere in the work place. This was seen as advantages as it reduces the potential for pin placement mishaps as a result of human error in placing the box. From this dynamic placement, the first objective of this project is using the computer vision to determine the global position of the pin holes, via the fixed position of the socket in the box, and the global position and orientation of the box in the work space.

The secondary objective is having the robotic arm collect a pin, and place it in the pin hole by converting the pinhole location in the camera frame to the required position in the robotic arm frame. The process for placing the pin with the robotic arm will then be as follows:

- Lower grasped pin halfway into hole
- Release pin
- Drive pin remaining distance into hole.

For this project, the confirmation of pins being ready in the supply is not being explored. This is due to the industry application being intended to use a vibrating bowl feed, and thus the assumption can be made pins will always be available. For this proof of concept, a rack of three pins is made, with the gripper positions being hard coded.

# Chapter 2

## Computer Vision

The computer vision of this project uses Open-CV for c++. This library contains many image-based functions for sourcing, manipulating, and presenting visual data. This library has been used for two roles, object detection, and robotic gripper required motion determination. Of these two task, the latter relies on the former.

### 2.1 Camera use

For this project, a basic 5 megapixel webcam was mounted above the work area. However, this was found to be insignificantly detecting pin-holes, as discussed below. To replace this camera, rather than purchasing an expensive high resolution webcam, this project make use of a HD camera already owned by most people. This is the rear-facing camera of most smart phones.

This project used the 13 megapixel camera of the OnePlus 2<sup>1</sup>. This video stream was fed to the system running the computer vision via the app *IP Webcam*<sup>2</sup>, which transferred a 1080pp video stream over the Swinburne Wi-Fi.

The phone was mounted over the work area via a 3D printed frame shown in fig. 2.1.

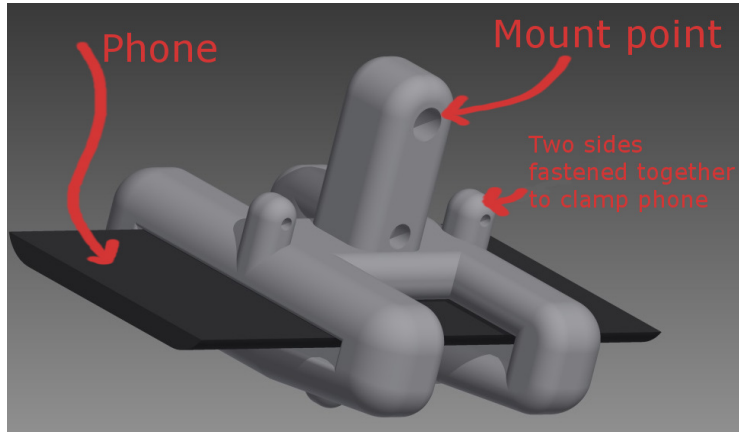


Figure 2.1: 3D printed phone mount.

### 2.2 Object detection

#### 2.2.1 Environment preparation

To begin the computer vision process a background image is taken when no objects are present. A keyboard control was added, 'Y', which allows a new background to be set. It was also added that this background was saved to file, so the system could be stopped, and restarted without needed to take a new background. However, it was advisable to take a new background every session, as lighting condition changes would cause issues with the object detection reporting false positives.

With the background set, a psudo-live stream of stills was captured from the camera. Each of these stills was then processed, as follows, before being discarded.

#### 2.2.2 Object recognition

The first step of processing was to do a raw matrix subtraction of the background. This gave an image of only the objects not in the background image. For this subtraction to function correctly, the background image needed to be free of all

<sup>1</sup><https://oneplus.net/2/camera>

<sup>2</sup><https://play.google.com/store/apps/details?id=com.pas.webcam&hl=en>

free-moving objects, as this subtraction would recognise a lack of object as well. An example of this subtraction is shown in fig. 2.2.

This image was then converted to a binary matrix, with a threshold of each colour layer, and a grey scale process, to combine the colour layers. This process is shown in fig. 2.3.

The resulting image was then eroded and dilated by one pixel layer. This erode function turns any white pixel touching to a black pixel into a black pixel, while the dilate function performs the opposite. This resulted in any small imperfections being removed from the image, while only slightly reducing the object recognition quality of the image. This is seen in fig. 2.4(a). A Canny edge detection was then used, which finds object edges by leaving only white pixels that are touching black pixels behind. The resulting image is shown fig. 2.4(b). Each group of remaining white pixels was now classified as a contour, via the *findContours* command. This process found any collection of white pixels as a polygon shape. It also listed the contour hierarchy, where contours are set as parents, and any contours inside its pixel range are defined as its children. The main holding box, and the gripper, are both objects not encased in larger objects. Therefore, only contours with no parents were further examined.

Each contour examined was fitted inside a rectangle with *minAreaRect*. This found the smallest rectangle, of any angular orientation, that could fit the whole contour. The size of this rectangle was then tested, anything outside the set threshold was ignored.

For each rectangle that was within the predicted size of the holding box or gripper, a classification and orientation was attempted as if the object were a holding box. If this process failed, the image was oriented as a gripper. If this failed, the object was deemed neither and discarded. From the example process, at the stage in fig. 2.4(b), three objects remain; the holding box, the gripper and another part of the gripper of no interest. Respectively, these objects would be assigned as a holding box; fail at being set as a holding box, and be assigned as a gripper, and fail at both assignments. This process is shown in diagram in fig. 2.5.

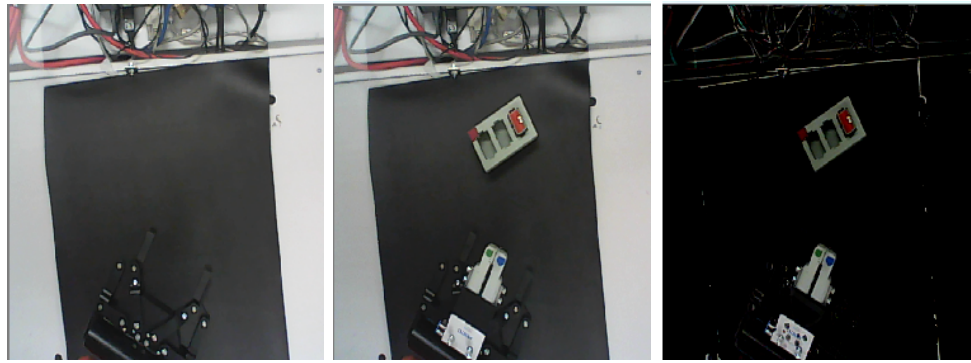


Figure 2.2: Background image, new capture with objects in place and resulting subtraction

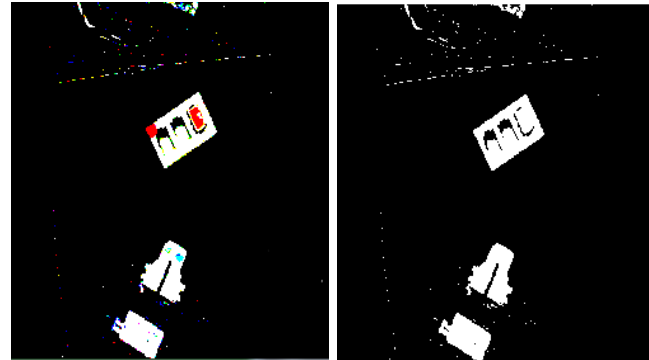


Figure 2.3: Threshold of each colour, and combining of colour layers to make single layer binary

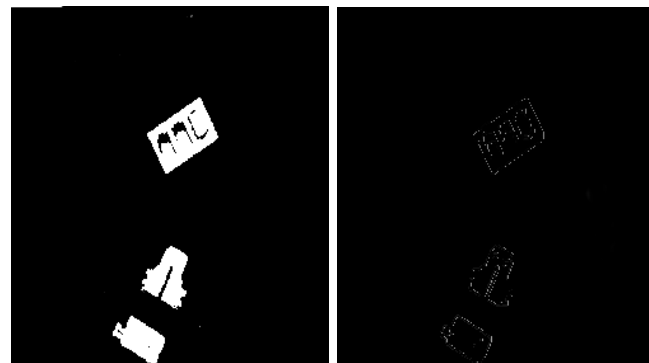


Figure 2.4: Erode and Dilate removes static from image, and Canny edge detection leaves only the outline of the objects



Figure 2.5: Assigning process through try, catch, throw

### 2.2.3 Object orientation

Both the holding box and gripper are recognised in this process as *RotatedRects* these are open-cv objects which consist of a size, angle and centre coordinate. However, the four corner points can be extracted from the object. When orientating as a holding box, each of these corners has the surrounding pixels examined, with the corner that has the highest ratio of red being deemed the reference corner. This reference corner is shown in figure fig. 2.6. To derive the highest red ratio eq. (2.1) was used. By referencing the corner with the most red *ratio* rather than highest red mean, a white corner is not incorrectly identified. If a corner of a set red ratio value is not found, the classification as a holding box is aborted, and a gripper is tried, as discussed above.

$$\text{mean(red)} / (\text{mean(blue)} + \text{mean(green)} + \text{mean(red)}) \quad (2.1)$$

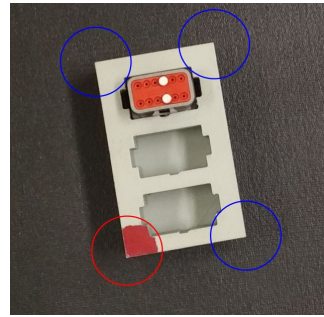


Figure 2.6: Red detection for reference corner

This reference corner was then used to determine the holding box true angle in relation to the camera. This is required as the angle of the *RotatedRect* is only in the range  $0^\circ$  to  $-90^\circ$ . Shown in fig. 2.7, the *RotatedRect* is initially a short, wide rectangle at  $-20^\circ$ . However, when rotated by  $-80^\circ$  the *RotatedRect* becomes a tall, thin rectangle at  $-10^\circ$ . To rectify this, the index of the reference corner from the list of corners returned from the *RotatedRect* function was examined, and the true angle was found with an addition of  $0^\circ$ ,  $90^\circ$ ,  $180^\circ$  or  $270^\circ$ .

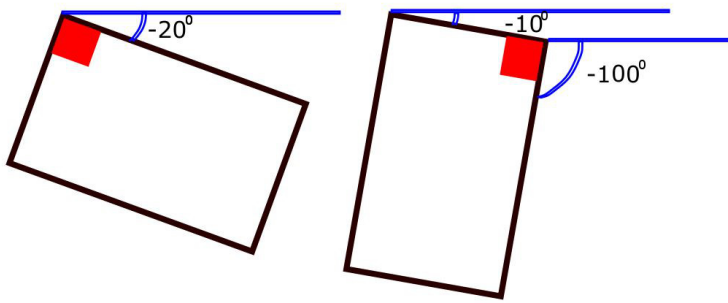


Figure 2.7

This orientation process is repeated for the gripper arm, but using the blue and green dots on the gripper fingers.

## 2.3 Pin detection and PinHole Allocation

With the holding box true angle determined, a copy of the image could be rotated and cropped to be only the holding box. This cropping can be seen in fig. 2.8. Data on this holding box could now be used to find the sockets in the holding box. This box information defines where the sockets should be (in millimetres), within the box. At this point, hard coding has been used, as only one holding box type

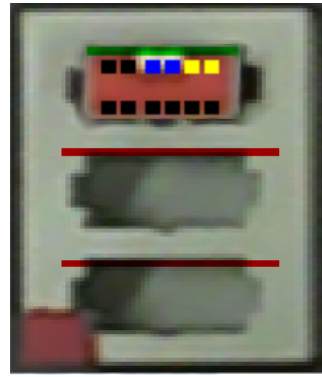


Figure 2.8: Holding box image, cropped down to only the box, and with all socket overlay shown

has been made. However if several holding boxes are used in future development, each box can have a simple, 4-bit bar-code like system, which allows the camera to detect which holding boxes are in the work area and access the socket information from an CSV file. An example of this bar-code is shown in fig. 2.9.

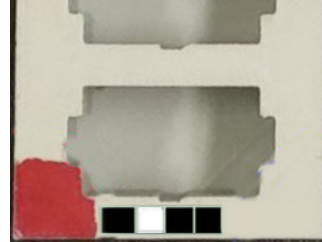


Figure 2.9: Example barcode with 0100, indicating the type of holding box.

By using the millimetres to pixel ratio, and the physical displacement of each socket, a *socket* object was made. Each socket object was passed the holding box image, its pixel starting point within this image, expected height, and file name for CSV file with pin details. The socket started by cropping a reference matrix of the box image to only the useful area. Using reference copies, or *shallow copies*, has two main advantages: Firstly, the memory used and copy execution time is reduced, as the socket's stored *Mat* is only a pointer, not a whole new matrix. Secondly, the socket image can be edited for user feedback, and the original holding box image is effected. This allows only a holding box to be presented to the user with all socket information being shown, rather than loading each socket image separately. An example of this is shown in fig. 2.8.

Using its sub-matrix, the socket examined the mean red ratios, as used for the holding box corner, and determines if a socket was present, as shown in fig. 2.10.

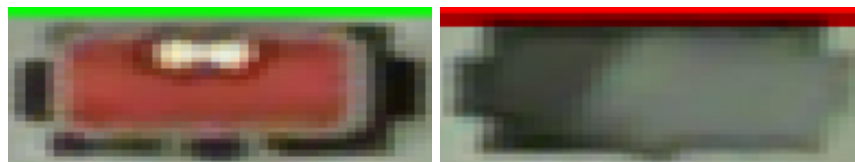


Figure 2.10: Active and empty socket place identified and presented with, respectively, green or red bar above

Sockets that have been identified as present are then further examined to find the exact area for pin hole mounting. Shown in fig. 2.11a is the original socket image. A threshold function of high red, low green, low blue is performed, fig. 2.11b. The image is eroded and dilated, fig. 2.11c, and a canny edge detection is conducted, fig. 2.11d. The image is then cropped to fit the resulting contour, fig. 2.11e.

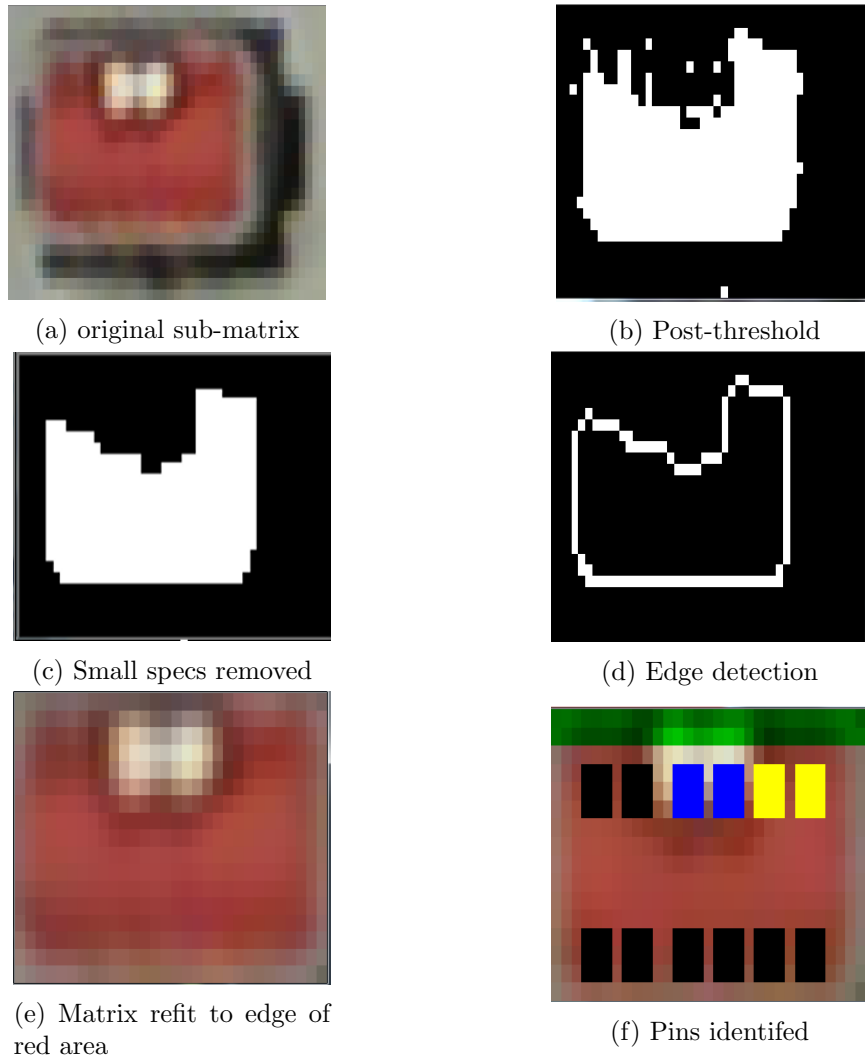


Figure 2.11: Image processing of socket

Using a CSV dataset, the locations of the pins is then assigned. The newly allocated pin hole is examined to find if a pin is present. To do this, the mean value of all three colour channels is compared with the 3 mean channels of the socket, if it is 25% greater, a (white) pin is determined to be present.

A second CSV file then provides information on which pin holes should be filled. The resulting pin layout is shown in fig. 2.11f, black pin holes are not filled, and should not be, blue have already been filled, and yellow still need to be filled. The holes which require filling are then further investigated. As seen in fig. 2.11f, the hole area is still large compared to the size of the pin. To reduce this area, and improve placement accuracy, the a sub matrix of only the pin hole area is made, ??, as seen in defining the socket above. This matrix is scanned for the least bright section. To do this each 3x3 pixel area is averaged, and the three colour channel means are summed together. The lowest area is then defined as the hole, with the centre of this area used as the pin hole pixel location.

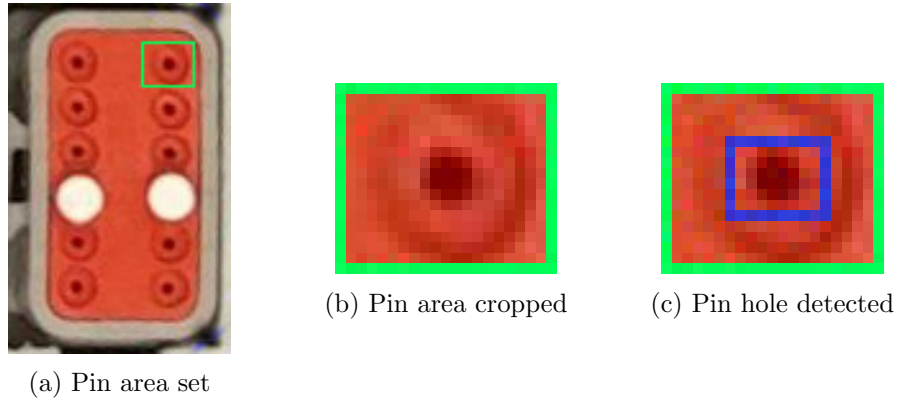


Figure 2.12: Pin hole identification. This example uses a high resolution image which is not feasible for video streaming, but is more presentable

## 2.4 Path creation

### 2.4.1 Pinhole and gripper location

With the pin holes assigned, the next available pinhole is requested from the main function. To do this, each layer between the main image and the pin holes are re-framed within their parent.

To begin, the first unfilled pinhole (coloured yellow above) reports to its parent socket the centre pixel location in the pin, combined with the location of the pin within the socket. The socket then combines this location, and the location of the socket within the parent holding box, and reports this value to its parent. The holding box then re-orientates this coordinate to the global frame, and combines it with the holding box's location in the global frame. This final, global position of the pin is then reported to the main function. A diagram of this process is shown in figure fig. 2.13.

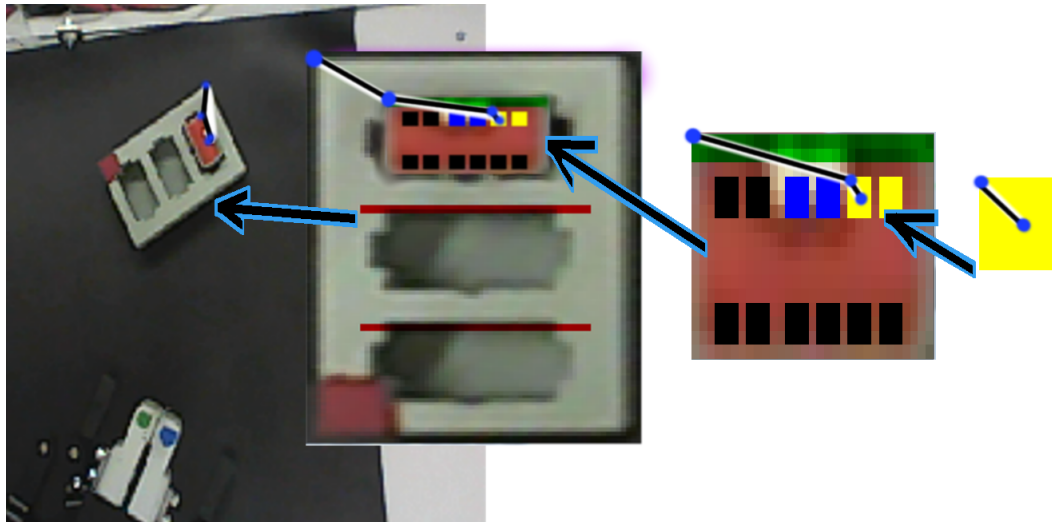


Figure 2.13: Local position, cascading to parent to find global pin position

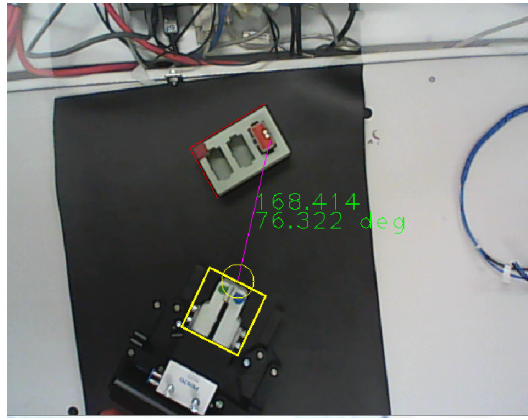


Figure 2.14: Gripper to pin hole vector display

To find a pixel singularity representation of the gripper, the half-way point between the blue and green corners, along the shared edge of the RotatedRect is reported to the main function.

#### 2.4.2 Measurement correction

As this application is being deployed under fluorescent lighting, there is some oscillation in recordings of the holing box and gripper. From this, the measurements recorded above cannot be assumed to be completely accurate. The graph shown in fig. 2.15 shows that if the above object detection process is repeated 30 times, in quick succession, and a vector is made from gripper pixel to pin-hole centre pixel for each recording, there is a range of values found.

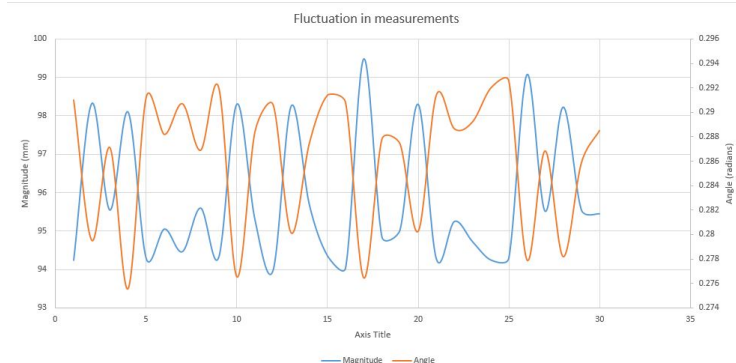


Figure 2.15: Vector magnitude and angle change over 30 records in close precession

To reduce this lighting issue, a collection of 30 location recordings are made. The mean, variation and standard deviation are found. The maximum and minimum values of these records, within 2 standard deviation of the mean, are then averaged to derive a value with some error tolerance. By using the minimum and maximum values only, a more accurate reading is made, as the video rate and light flicker rate may be at a difference that even distribution of recordings is not made. The standard deviation restriction is used so a minimum or maximum value which represents a recording error is less likely to be used, as it would be an outstanding outlier.

#### 2.4.3 Path to gripper arm co-ordinates

To move the gripper towards its target pin-hole destination for placement, the robot-frame position of the pin hole must be known. To find this, the vector from gripper to pin hole in the camera frame, found above, is broken down into Cartesian components and transformed into robot-space.

The following assumptions about the camera and workspace were made to simplify the design of the pixel to robot-frame conversion.

- No camera distortion is present
- The effects of field-of-view and perspective are ignored due to the heads-down and mainly depth-agnostic nature of the workspace
- The z-position of target pin-hole is constant and known

Before the conversion can be made, a configuration measurement must be performed to create a vector  $X_c$ , aligned to the x-axis of the robot-frame, within the camera-frame. This is done by recording the camera-frame location of the gripper at the robot home position, and after moving the gripper 200mm along the x-axis of the robot-frame, using the measurement correction method of section 2.4.2. This allows for decomposition of the gripper-to-pin-hole vector  $P_c$  into terms of perpendicular vectors  $X_c$  and  $Y_c$  (y axis). To find these  $P_c$  components the following equations are used.

$$P_{cx} * X_c = (X_c \cdot P_c) / (|X_c| |X_c|) X_c \quad (2.2)$$

$$P_{cy} * Y_c = P_c - P_{cx} * X_c \quad (2.3)$$

These vectors are the pixel space components aligned to world-space axis. To obtain the world-space scaled vector of the pin-hole  $P_w$ , the constants  $P_{cx}$  and  $P_{cy}$  are multiplied by the pixel to world scaling factor (200mm / the magnitude of  $X_c$  (pixels)). The gripper can now be commanded to move the transformed world pin-hole vector,  $P_w$ , for placement of the pin.

#### 2.4.4 Error correction

After adapting the system to use a HD camera, errors in the conversions to robot-frame positions were observed, as seen in fig. 2.16(a).

The green dots are the expected robot-frame locations,  $X_n$ , and the red lines are the error vectors,  $Err$ , a vector from  $X_n$  to the calculated estimate position,  $M_n$ , with magnitude scaled by 10 for observation purposes. The value for  $Err$  is derived from eq. (2.4)

$$10(Err) = 10(X_n - M_n) \quad (2.4)$$

This error has been observed to be due to the field-of-view of the camera, causing perspective and radial image distortion. To remedy this, a correction function was applied to the calculated target pin locations in relation to the distance to the camera focal point  $F$ . The corrected location is thus calculated by:

$$CorrectionFactor = (\alpha)|F - M_n| + (\beta)(sigm(F - M_n))|F - X_n|^2 \quad (2.5)$$

$$CorrectedPoint = InputPoint - CorrectionFactor \quad (2.6)$$

where  $\alpha$  and  $\beta$  are user set constant, which relate to the observed distortion of the camera.

The amount each calculated point is corrected is quadratically dependent on its position in relation to a selected global focal point. Initially, the constants  $\alpha$ ,  $\beta$  and  $F$  were chosen by using a GUI application, allowing the user to experiment by manually setting the focal point via clicking inside the image, and inputting values for  $\alpha$  and  $\beta$ . An example of the improvement obtained by this approach is shown in fig. 2.16(b). The cyan dots are the error vectors observed after correction, and the white dot is the focal point. This design results in a notable increase in overall accuracy, and the ability to mitigate all error in a small target area by selecting appropriate constants.

To reduce the manual calibration process during set-up, the focal point positioning was automated by using a known position. This automation process did not alter the  $\alpha$  or  $\beta$  values, as these are seen to remain constant for the camera.

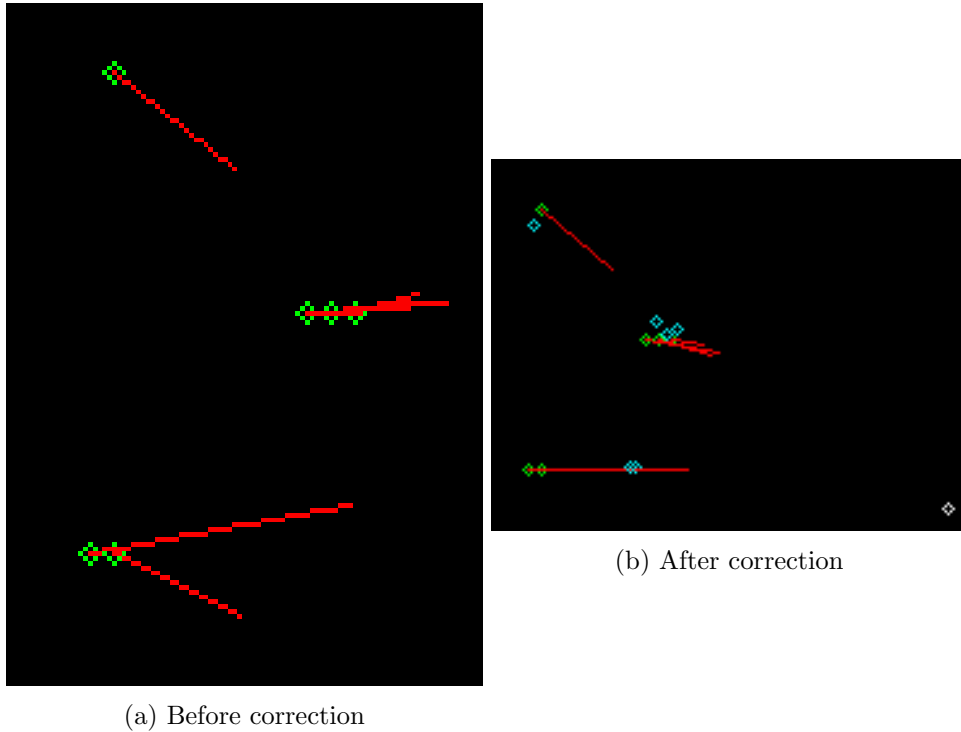


Figure 2.16: Dipiction of magnitude (x10) and direction of measurement errors, observed for calculated robot-frame positions.

To begin, the robotic arm was manually driven to a position 150mm on both the x and y axis in the robotic-arm frame. The holding box was then placed in such a position that the first allocated pin was at this gripper tip location.

The robotic arm was returned to the home position, and the object detection and camera frame to robot-arm frame conversion was preformed. The resulting conversion was then passed through the above error correction, with a focal point at  $x=0\text{mm}$ ,  $y=1000\text{mm}$  from home. The focal point was then adjusted on the x and y axis based on the difference from the error correction output from the expected output of  $x=150\text{mm}$ ,  $y=150\text{mm}$ .

This process was repeated until the error correction resulted the expected output, with a tolerance of 0.5mm.

## 2.5 Camera future development suggested

The current camera system requires some manual calibration adjustments, is recording a large about of the unused work space, and loses pin-hole detection ability when the robotic arm moves over the holding box. To improve the camera accuracy it is suggested that a low resolution camera is used for work space analyses to detect the holding box. A second camera may then be mounted on the robotic gripper for a close-range socket analyses, and pin-hole detection. This would allow the gripper to find the pin hole, with a much lower camera view distortion, and would allow the arm to make final potion adjustments with camera feedback during placement.

# Chapter 3

## Robotic Arm Control

### 3.1 Open ABB

For this project, a basic parallel port was available for communication between the computer vision and the robotic arm. The parallel port allowed for single bits to be used as flags which triggered the robotic arm to perform action sets. For this project we needed to send specific travel destinations from the computer vision, to the robotic arm, therefore a more advance communication was required. To achieve this, OpenABB<sup>1</sup> was used. This system has the robotic controller running a basic TCP server via RAPID code. A python script is used on the computer to connect to this server, and send commands. One such command can move the gripper to any point in the arm's reachable workspace, by sending the three axis coordinates. This command list was extended by the team to include gripper control and moving about the x and y axis, relative to the current position, while holding the z axis value. An example of the command stack is shown in fig. 3.1.

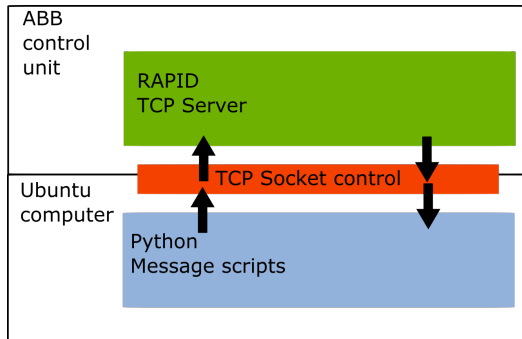


Figure 3.1: Communication layers of OpenABB

### 3.2 Coordination

As the computer vision was made in c++, and the openABB c++ code requires a full ROS installation, it was instead chosen to implement a python calling system in c++. This interface called a python run-time, and sent commands via *PyRunSimpleString*.

The command stack was thus extended as shown in fig. 3.2

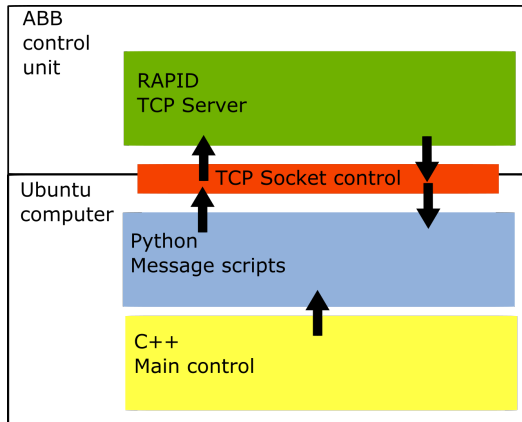


Figure 3.2: Communication stack with added c++

<sup>1</sup><https://github.com/robotics/openabb>

### 3.3 Pin placement operation

As the pin needed to be fully pressed into the hole two sub operations were required for the pin placement; first, the gripped pin was driven as far into the hole as possible, while having the gripper not damage the socket. The gripper was then raised, and the flat surface of the gripper pressing the pin the remaining depth into the hole. This process is shown in fig. 3.3

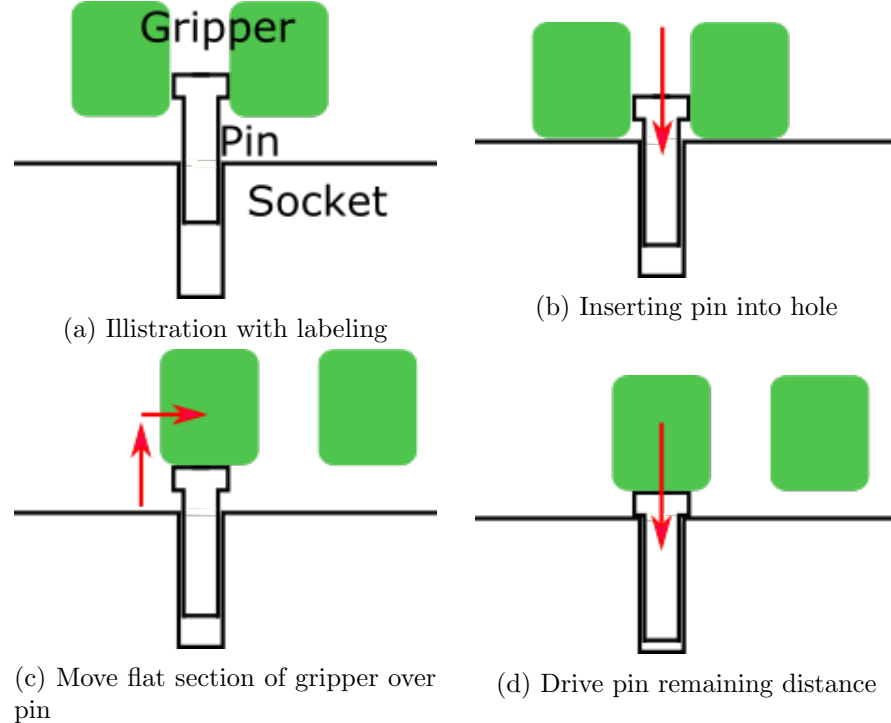


Figure 3.3: Pin placement illustration

## Chapter 4

# Operation Flow

With the system's ability to know where to move to, and the ability to coordinate these movements, the operation flow charts can now be presented. Fig. 4.1 shows the standard operation flow, with purple action points being computer vision processes, and pink being robotic arm actions. Fig. 4.2 shows the operation for calibrating the difference between robotic arm frame, and the camera frame.

From fig. 4.1 it can be seen that the gripper returns to the 'zero' position and restarts pin hole measurements after each pin placement. This flow was chosen over calculating all hole positions and making all motion in one round, as each pin placement may move the holding box a small amount. This would result in all further pin placements being incorrect and pins not entering the correct holes.

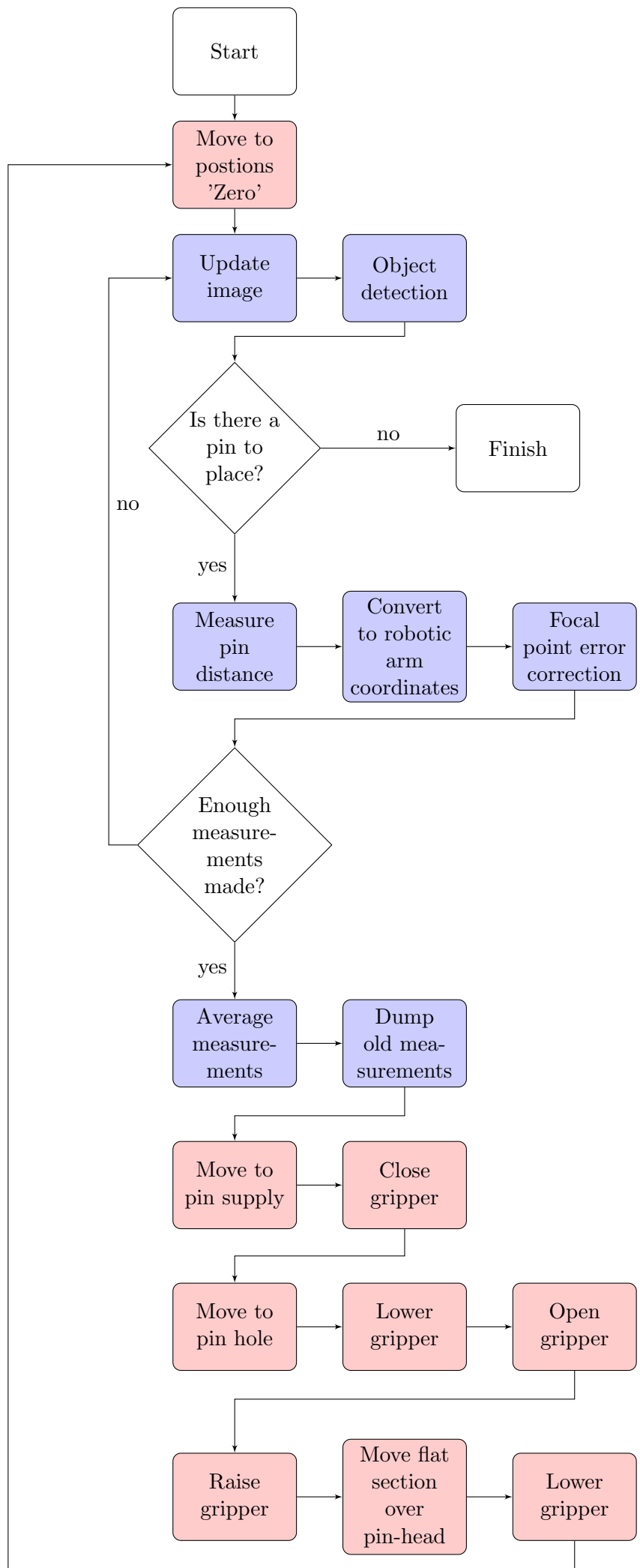


Figure 4.1: Main Process

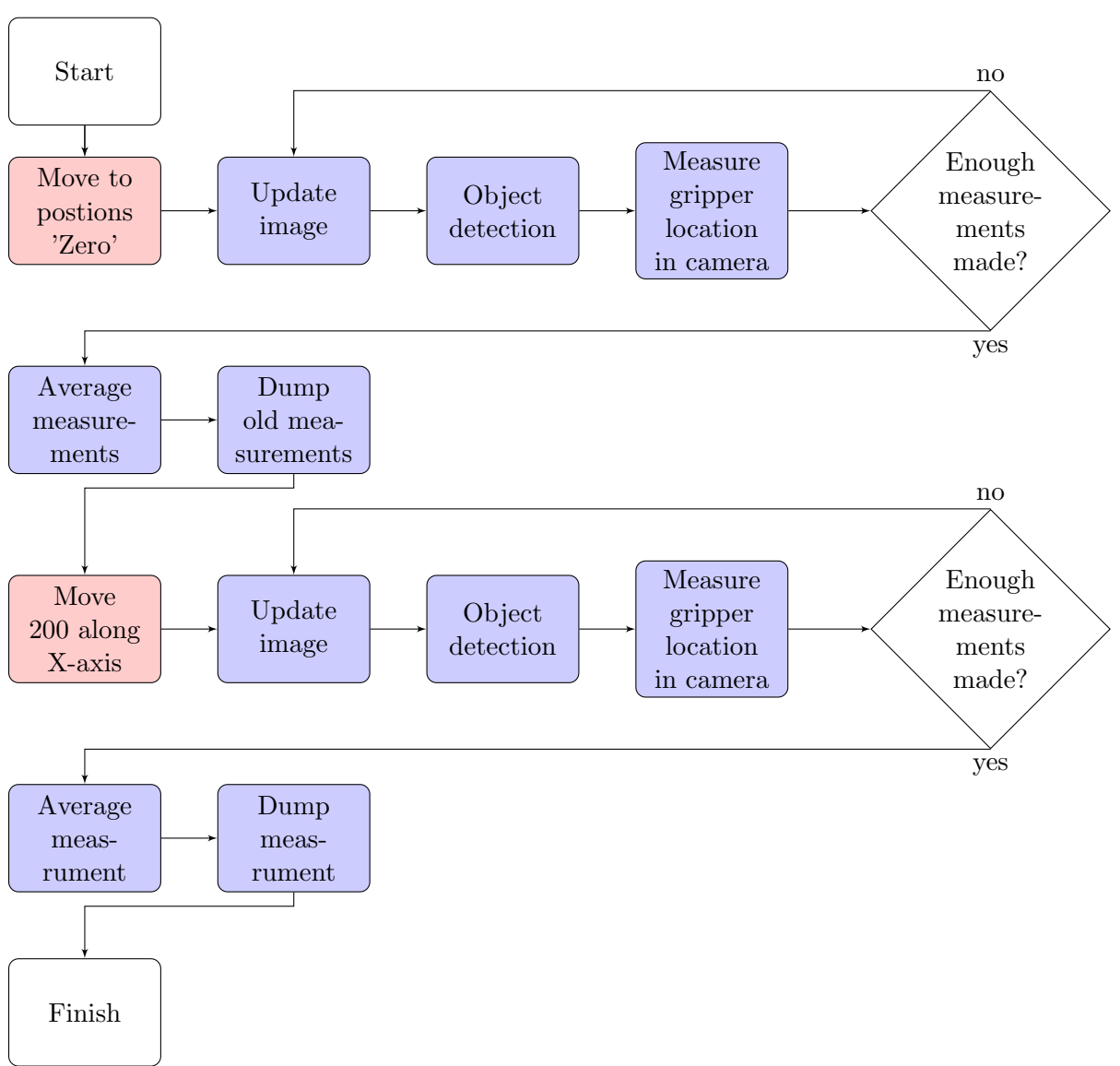


Figure 4.2: Calibration

# Chapter 5

## Matlab Simulation

### 5.1 Denavit-Hartenberg Algorithm

| Links | $\theta$   | d     | a    | $\alpha$ | Physical |
|-------|------------|-------|------|----------|----------|
| 1     | $\theta$   | 0     | 0    | 0        | Base     |
| 2     | $\theta_2$ | 0     | 0.07 | $\pi/2$  | Shoulder |
| 3     | $\theta_3$ | 0     | 0.36 | 0        | Elbow    |
| 4     | $\theta_4$ | 0.38  | 0    | $\pi/2$  | Twist-1  |
| 5     | $\theta_5$ | 0     | 0    | $-\pi/2$ | Wrist    |
| 6     | $\theta_6$ | 0.108 | 0    | $\pi/2$  | Twist-2  |

Table 5.1: Denavit-Hartenberg Algorithm

The Denavit-Hartenberg matrix above gives a close approximation to the movement and joint rotation behaviour of the ABB robot arm. Due to the nature of elbow and wrist rotations, a ‘d’ offset is given for joints 4 and 6, allowing a rotation about the length of a previous link.

Assumptions are made with the position of joints 4 and 6, where joint 4 is located roughly in the middle of joints 3 and 5 on the physical robot, however since it’s rotation is about the link axis it is irrelevant where this joint is located, so long as it is within the linkage length. That is to say, if this link is rotated by a joint at any point along its length, the rotational behaviour of further joints will be the same. Due to this behaviour, joint 4 can be simulated at one end of the robot’s forearm, instead of at its physical location on the robot’s forearm.

A problem occurs when attempting to set a joint which rotates about the link axis. When the Matlab link configuration has an ‘a’ or ‘d’ offset after any joint which rotates about a link axis, Matlab cannot construct the robot arm model correctly in the simulation. This is due to the ‘a’ and ‘d’ offset lengths both being perpendicular to the link axis. In order to fix this problem and simplify the Denavit-Hartenberg algorithm, it is easier to set the distance between joints 4 and 5 to zero then rotate joint 5 into the correct orientation.

It was also assumed that joint 6 can be located at the end-effector in order to benefit the simulation so that movements and translations will include that distance in calculations. This means that the link between joints 5 and 6 will simulate the end-effector.

Regardless of alterations made in order to simplify the algorithm notation or fix errors produced in a Matlab simulation, the motion characteristics are equivalent to the physical movements of the ABB robot.

### 5.2 Matlab implementation

The Matlab Robotic, Vision and Control library (RVC) is useful for mathematically representing configured links on a robot arm using Denavit-Hartenberg notation. When using the algorithm, links can be created by a user and added to a defined Robot object using the SerialLink() function.

A single position may be mapped using an array of elements equal to the amount of links. Each element represents either joint translation for prismatic joints or rotation for rotary joints. The order in which the joints are represented in the array need to be the same order in which the links were created in the Denavit-Hartenberg algorithm. For the ABB robot, only rotational joints are present.

To begin with, a starting position is defined for the robot arm joint rotation, in this case all angles are set to zero degrees, which represents the unmodified model of the Denavit-Hartenberg algorithm. In this pose it is easy to see whether or not

screenshot

the joints are configured correctly and that the model does in fact mirror the basic shape of the physical model being simulated.

The next step is to define the x,y,z position and rotation for each point of motion which will be simulated. This can be done by simply assigning variables to represent that information as in appendix A, lines 44-105. In order to run an effective simulation, the position and rotations must be compiled into a transformation matrix. This matrix defines all translational and rotational movement required between the reference frame and the desired destination frame. In order to convert the raw variables representing the position and rotation of the end-effector into a transform matrix, two functions are used; one is  $transl(x,y,z)$ , which represents translation and takes in the x, y and z position of a point, and the other is  $rpy2tr(rx,ry,rz)$ , which represents the roll, pitch and yaw angle, which rotate about x, y and z respectively. The result of these two functions are multiplied together and saved as the transformation matrix for the specified point, in the order as seen in appendix A, lines 107-114. A transformation matrix for the initial position is also required. This is achieved easily by using the forward-kinematic function  $fkine(q)$ , where  $q$  is a  $1 \times n$  array representing the joint rotations with  $n$  being the number of joints on the robot arm.

In appendix A, lines 120-126, two arrays are initiated. The first is a mask representing the degrees of freedom available in the joint path calculations. The latter is a joint angle position array which acts as a reference point. This point is useful by forcing the movement of the arm to conform to the specified joint angles. This helps to simulate movement that stays within the bounds of the work area of the robot. As a solution for each joint converges with the corresponding reference angle, the angles will only change when a joint has the least convergence.

Although there is a transformation matrix for each position that will be simulated, what is actually required is the joint angle values, in radians, which are the exact rotations of each joint. These together correspond to the position of the end-effector. In order to get such an array from a transformation matrix, the inverse-kinematic function  $ikine(T,qr,M)$  can be used, where  $T$  is a transformation matrix for the point,  $qr$  is the reference array used to restrict motion and  $M$  is the mask for the degrees of freedom available. For the ABB robot, the joint angles at the simulated points are calculated as in appendix A, lines 120-135. When finding the inverse kinematic of the transformation matrix, the function  $ikine()$  takes into account the reference array and the degrees of freedom in order to find a single solution for the joint angle configuration which makes up the desired position and rotation. Users must be careful, however, as having an inappropriate reference array may cause the calculations to diverge, resulting in sub-optimal solutions which may even result in simulation movement outside of the immediate work area.

# Appendix A

## Matlab Code

```
1 % Simple example of using the Matlab Robot toolbox v9.9 for RME40003 Robot
2 % Systems Design , 2014.
3 %
4 % The example is for a three-link RPR manipulator that was covered in the
5 % lectures and the tutorials .
6 %
7 % Example developed by M. Dunn, 2014, Swinburne University of Technology ,
8 % Melbourne , Australia
9 %
10 % References :::
11 % - Robotics , Vision & Control , Chap 7
12 % P. Corke , Springer 2011.
13
14 clear L
15
16 %% Define the link parameters for the manipulator
17 % Set the fifth parameter as 0 for a rotary joint , 1 for a prismatic joint
18 % Set the "modified" flag to true (we are using the modified
19 % Denavit-Hartenberg convention in RME40003)
20
21 sF = 1.0;
22 %
23 L(1) = Link([ 0 0 0 0 0], 'modified');
24 L(2) = Link([ 0 0 0.07 -pi/2 0], 'modified');
25 L(3) = Link([ 0 0 0.36 0 0], 'modified');
26 L(4) = Link([ 0 0.38 0 -pi/2 0], 'modified');
27 L(5) = Link([ 0 0 0 pi/2 0], 'modified');
28 L(6) = Link([ 0 0.108 0 -pi/2 0], 'modified');
29
30 %% Set up the manipulator
31 robot = SerialLink(L, 'name' , 'RME40003 Project ');
32
33 %% Define some poses
34 %start pose
35 q0 = [ 0, -pi/4, -pi/4, 0, 0, 0];
36
37 % 1:Base-rot
38 % 2:shoulder-rot
39 % 3:elbow-rot
40 % 4:elbow-twist
41 % 5:wrist-pivot
42 % 6:wrist-twist
43
44 %% Raw position and rotation data for each point
45 %point1
46
47 x1 = 0.273/sF;
48 y1 = -0.740/sF;
49 z1 = 0.02/sF;
50
51 %radians
52 rotx1 = pi;
53 roty1 = 0;
```

```

54 rotz1 = 0;
55
56 %point2
57 x2 = 0.273/sF;
58 y2 = -0.740/sF;
59 z2 = -0.1/sF;
60
61 %radians
62 rotx2 = pi;
63 roty2 = 0;
64 rotz2 = 0;
65
66 %point3
67 x3 = 0.273/sF;
68 y3 = -0.740/sF;
69 z3 = 0.02/sF;
70
71 %radians
72 rotx3 = pi;
73 roty3 = 0;
74 rotz3 = 0;
75
76 %point4
77 x4 = 0.4/sF;
78 y4 = -0.4/sF;
79 z4 = 0.02/sF;
80
81 %radians
82 rotx4 = pi;
83 roty4 = 0;
84 rotz4 = 0;
85
86 %point5
87 x5 = 0.4/sF;
88 y5 = -0.4/sF;
89 z5 = -0.1/sF;
90
91 %radians
92 rotx5 = pi;
93 roty5 = 0;
94 rotz5 = 0;
95
96 %point6
97 x6 = 0.4/sF;
98 y6 = -0.4/sF;
99 z6 = 0.02/sF;
100
101 %radians
102 rotx6 = pi;
103 roty6 = 0;
104 rotz6 = 0;
105
106
107 %% Point translation homogeneous matrixes
108 T1 = transl(x1,y1,z1)*rpy2tr(rotx1,roty1,rotz1);
109 T2 = transl(x2,y2,z2)*rpy2tr(rotx2,roty2,rotz2);
110 T3 = transl(x3,y3,z3)*rpy2tr(rotx3,roty3,rotz3);
111 T4 = transl(x4,y4,z4)*rpy2tr(rotx4,roty4,rotz4);

```

```

112 T5 = transl(x5,y5,z5)*rpy2tr(rotx5,rotY5,rotz5);
113 T6 = transl(x6,y6,z6)*rpy2tr(rotx6,rotY6,rotz6);
114
115
116 %% Find the forward kinematics of the pose
117 fk_q0 = robot.fkine(q0);
118
119
120 %% Find the inverse kinematics for fk_qs and fk_qe
121 % Set a mask for the degrees of freedom
122 M = [1, 1, 1, 1, 1, 1];
123
124 % Point set for forced convergence
125 qi = [0, -pi/4, -pi/4, 0, pi/2, -pi/2];
126
127 % Calculate the inverse kinematics of each point
128 ik_q0 = robot.ikine(fk_q0, qi, M); %fk of initial angles, initial position
    estimation, DOF settings
129 ik_q1 = robot.ikine(T1, qi, M);
130 ik_q2 = robot.ikine(T2, qi, M);
131 ik_q3 = robot.ikine(T3, qi, M);
132 ik_q4 = robot.ikine(T4, qi, M);
133 ik_q5 = robot.ikine(T5, qi, M);
134 ik_q6 = robot.ikine(T6, qi, M);
135
136 %% Find the joint trajectory for ten steps between the two poses
137 % Set the number of points
138 num_points = 10;
139
140 % Moving from point to point
141 jt0_1 = traj(ik_q0, ik_q1, num_points);
142 jt1_2 = traj(ik_q1, ik_q2, num_points);
143 jt2_3 = traj(ik_q2, ik_q3, num_points);
144 jt3_4 = traj(ik_q3, ik_q4, num_points);
145 jt4_5 = traj(ik_q4, ik_q5, num_points);
146 jt5_6 = traj(ik_q5, ik_q6, num_points);
147 jt6_0 = traj(ik_q6, ik_q0, num_points);
148
149 % Set the workspace of the robot
150 robot.plotopt = { 'workspace', [-1, 1, -1, 1, -1, 1] };
151
152 % Plot the animations
153 while 1
154     robot.plot(jt0_1);
155     pause(1);
156     robot.plot(jt1_2);
157     pause(1);
158     robot.plot(jt2_3);
159     pause(1);
160     robot.plot(jt3_4);
161     pause(1);
162     robot.plot(jt4_5);
163     pause(1);
164     robot.plot(jt5_6);
165     pause(1);
166     robot.plot(jt6_0);
167     pause(1);
168 end

```